Damage monitoring of refractory wall in a generic entrained-bed slagging gasification system

S Chakraborty, S Sarkar, S Gupta, and **A Ray***
Mechanical Engineering Department, Pennsylvania State University, PA, USA

The manuscript was received on 18 May 2008 and was accepted after revision for publication on 22 July 2008.

DOI: 10.1243/09576509JPE638

Abstract: The main cause of performance degradation in entrained-bed slagging gasification systems is attributed to evolution of structural damage in the refractory walls. Early detection of such damage is necessary to avert unscheduled shutdown of a gasification plant. This paper develops an integrated computer simulation model of a generic entrained-bed slagging gasifier for formulation of a damage prediction algorithm with the objective of real-time degradation monitoring and condition-based maintenance of refractory walls. The integrated simulation model yields: (a) quasi-steady-state spatial temperature profiles at any cross-section of the gasification system, and (b) dynamic response of the refractory wall temperature that is measured by an array of sensors installed at specified locations on the external surface of the gasifier wall. The key idea for early detection of refractory-wall damage is built upon the fact that a local anomaly (i.e. deviation from the nominal condition) is likely to influence the temperature gradient in the refractory wall due to changes in the thermal impedance. The information from dynamic response of refractory temperature is extracted in a compressed form as statistical patterns of evolving anomaly through usage of a recently reported data-driven pattern identification tool called symbolic dynamic filtering (SDF). The results of this model-based investigation show that the proposed anomaly detection and damage prediction method is potentially capable of characterizing the health status of refractory walls in particular and the entire gasification system in general. The SDF algorithms in this paper are implemented on the MATLAB platform and are interfaced with the gasification plant simulation model for emulation of real-time degradation monitoring.

Keywords: entrained-bed slagging gasification systems, refractory failure, fault diagnostics, time series data analysis

1 INTRODUCTION

Modern day gasification plants offer a versatile and clean way to convert coal and other alternative fuels into electricity, hydrogen, and a variety of readily usable energy products [**1**]. Instead of directly burning the fuel, a gasification plant chemically breaks down the feedstock into its basic constituents. For example, a carbon-based feedstock (e.g. coal) is typically exposed to hot steam and carefully controlled amounts of air or oxygen at high temperatures and pressures. Carbon molecules in the feedstock break apart and set off a chain of chemical reactions that typically produce a mixture of carbon monoxide, hydrogen, and other gaseous compounds [**1**].

The key component of a gasification plant is the gasifier that converts feedstock into gaseous constituents. However, a gasifier differs from a conventional combustor in the sense that it allows for only *partial oxidation* that breaks down most of the carbon-containing feedstock to produce the *syngas* [**2**]. The syngas is essentially a mixture of hydrogen (H_2), carbon monoxide (CO), and other gases; their proportions may vary depending upon the conditions in the gasifier and the type of feedstock. Gasification-based electric power plants are now operating commercially in the United States and in other countries [**1**]. It is predicted

**Corresponding author: Mechanical Engineering Department, Pennsylvania State University, 329 Reber Building, University Park, PA 16802, USA. email: axr2@psu.edu*

that gasification will be a major source of clean-fuel technology (e.g. US Department of Energy's FutureGen prototype advanced coal gasifier [**1**]) for several decades into the future. A major challenge in this endeavour is to ensure safe and reliable operation of gasification systems, specifically, prediction of (possibly distributed) structural damage and quantification of structural integrity in the gasifier wall.

Although much research and development effort has been expended to improve the refractory materials that can resist slag penetration and survive longer in the adverse operational environments of gasifiers, the life span of refractory walls in laboratory-scale gasifiers has been found to be short and widely fluctuating (e.g. approximately in the range of 4–14 months). Two dominant refractory failure mechanisms include (a) chemical dissolution and (b) fatigue damage in the material microstructure. If unchecked, these faults evolve in time to cause loss of performance and possibly unscheduled shutdown of the plant. Hence, early detection of incipient damage in the refractory walls is a critical issue in the gasification industry.

The above discussions evince that it is necessary to develop real-time diagnosis tools with capabilities of generating early warnings as needed for the maintenance of gasifiers to enhance their service life. Current state-of-the-art in degradation monitoring of entrained-bed slagging gasifiers provides a variety of fault diagnostic methodologies that are primarily built upon microstructural analytical models of damaged refractory bricks [**3**] apparently without taking advantage of sensor-based analytical tools. It is necessary to address these issues from the perspectives of condition-based maintenance (CBM) that requires advanced tools of degradation monitoring and must be capable of real-time detection and information-based intelligent decision-making and control [**4**].

This paper presents the development of an integrated simulation model of a generic entrained-bed slagging gasifier for formulation of a damage detection procedure with the objective of real-time degradation monitoring and (CBM) of refractory walls. The simulation model integrates the mechanisms of gasifier kinetics, slag formation and flow, and heat transfer through the refractory wall. The integrated model yields steady-state spatial temperature profiles at any cross-section of the gasification system as well as dynamic response of the refractory wall temperature that is measured by an array of sensors installed at different axial locations on the external surface of the gasifier wall. The key idea for early detection of refractory-wall damage accrues from the fact that a local anomaly (i.e. deviation from the nominal condition) is likely to influence the temperature gradient in the refractory wall due to a change in the thermal impedance.

A variety of statistical pattern recognition tools have been reported in references [**5**] and [**6**] for fault detection and estimation in dynamical systems. This paper has adopted a recently reported data-driven pattern identification technique called symbolic dynamic filtering (SDF) [**4**, **7**, **8**] that enables compression of information into pattern vectors of low dimension; the theory of SDF is succinctly reviewed in Appendix 2. Specifically, this paper shows how to extract information from the sensor data and/or response of the gasification model in a compressed form as statistical pattern of the evolving damage using the concepts of SDF. Recent literature has reported experimental validation and efficacy of SDF in various applications, such as fatigue damage detection in structural materials [**9**, **10**] and impending failures in active electronic circuits [**11**, **12**].

From the perspectives of real-time damage detection and CBM of the refractory wall of a gasifier, the major contributions of the paper are delineated below.

1. Integrated simulation modelling of a generic entrained-bed slagging gasification system for formulation of a degradation monitoring algorithm.
2. Statistical pattern analysis of sensor time-series data in combination with the integrated simulation model for damage detection and failure prediction.

The paper is organized as follows. Section 2 explains the degradation mechanisms in the refractory wall of a gasifier. Section 3 provides details of the simulation model. Section 4 describes the proposed method for degradation monitoring, which involves dynamic modelling of the refractory wall and placement of sensors on the external surface of the gasifier. Section 5 presents the simulation results including possible failure scenarios. Finally, the paper is summarized and concluded in section 6 along with recommendations for future research. Appendix 2 briefly reviews the underlying concepts and salient features of SDF [**4**] that has been adopted for robust detection of incipient damage in the refractory wall.

2 DEGRADATION MECHANISMS IN REFRACTORY WALLS

Two inter-dependent damage mechanisms that cause degradation in the refractory wall of an entrained-bed slagging gasifier, leading to gradual failure and unscheduled shutdown, are explained below.

1. *Chemical dissolution of the refractory material.* This phenomenon is caused due to penetration of slag through the porous structure of the refractory wall that reacts and chemically dissolves the refractory material.

2. *Fatigue damage from growth of microstructural cracks*. This phenomenon is caused due to thermal fluctuations and interstitial pressure that develops from differential expansion between the refractory material and the slag. This leads to gradual development of several microstructural cracks inside the refractory surface, which eventually merge together into a single large crack causing rapid failure.

Slag penetration is the root cause of the above damage mechanisms that gradually degrade the refractory lining and lead to bulk removal of the material of refractory walls at random discrete intervals of time; this phenomenon is called *spalling* [**13**, **14**]. The chemical dissolution of refractory walls due to slag penetration weakens the material properties and also leads to crack initiation by creating several crack sites due to irregular dissolution of the material. This phenomenon causes fatigue crack initiation and also enhances fatigue crack propagation due to local weakening of the refractory materials. Fatigue crack growth leads to further slag penetration that, in turn, causes more chemical dissolution. The interdependence of these two phenomena has not been adequately modelled in the current state-of-the-art. Even with the simplifying assumption that they are independent of each other, the process of damage evolution in refractory walls of slagging gasifiers is a complex stochastic phenomenon due to unknown slag penetration and reaction mechanisms through porous medium of the refractory. Therefore, the development of detailed failure models has not been addressed in this paper and is beyond the scope of this investigation.

The purpose of the present investigation is the detection of refractory wall damage through statistical analysis of observed time-series data, rather than accurate modelling of failure mechanisms. For the purpose of damage detection and monitoring, the pertinent information of failure characteristics in refractory walls (e.g. time to failure and average spalling depth), reported from laboratory experiments and field studies [**13**], has been incorporated in the simulation model (see section 4). In essence, the objective of this paper is *in situ* damage monitoring of the refractory walls by time-series analysis of temperature response and compressing the relevant information into statistical patterns of evolving damage.

Once a refractory undergoes degradation, the deteriorated refractory structure affects the gas-path and the slag-refractory-heat transfer models. The change in the boundary condition of heat transfer and temperature distribution also affects the chemical-kinetics, which in turn leads to a new thermochemical equilibrium condition for the entire gasification system. In this altered equilibrium, the temperature profile could be significantly different from the original. Both steady-state spatial distributions of temperature and dynamic characteristics of the temperature profiles undergo different types of changes that become an important clue for detection and identification of an anomalous plant condition.

3 SIMULATION MODEL OF GASIFICATION SYSTEM

Technical literature provides ample information on modelling and analysis of various aspects of coal gasification. Computational fluid dynamic (CFD) analysis for both gas-path [**15**, **16**] and slag flow has been reported independently and extensive literature exists on modelling of stress distribution and thermal failure of refractory materials [**17**, **18**]. Apparently, the current state-of-the-art does not provide any reliable integrated model of the entrained-bed slagging gasification system for online damage monitoring in the refractory walls. Since the present paper focuses on real-time degradation monitoring in refractory materials, an isolated CFD model of gas-path dynamics may not be adequate due to insufficient information on slag flow and heat transfer and due to its computational overhead and complexity. Therefore, an integrated model is required to generate time series of fluctuations in process variables (e.g. gas and refractory wall temperatures) at different spatial locations. A quasi-steady-state model suffices for the gas-path while the dynamics could be extraneously incorporated in the heat transfer model of the refractory wall as explained below. As shown in Fig. 1, a simulation model of the gasification system is constructed by integrating the models of the following subsystems:

(a) gas-path kinetics;
(b) slag flow;
(c) heat transfer through the slag-refractory wall.

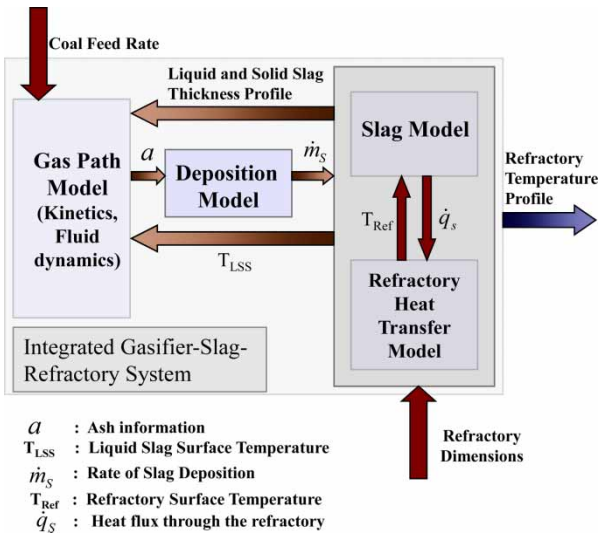

Fig. 1 Gasification system model architecture

The following subsections present the development of an integrated model of an entrained-bed slagging gasification system. Before proceeding to modelling details, a concept of three time scales is presented.

3.1 Concept of three time scales

The gasification system incorporates three different time scales in the mechanisms of (a) gas-path kinetics, (b) heat transfer through the interface of slag-refractory wall lining, and (c) evolution of damage in the refractory wall, respectively. The gas-path dynamics with its relatively fast response can be clearly separated from the refractory thermal characteristics that have a relatively sluggish response due to its large thermal mass and capacitance. For a disturbance in the operating conditions, whether intentional or unintentional, the fast gas dynamics quickly respond to the changes and attain a new steady state; this change in the gas-path may appear only as new boundary condition to the slag-refractory model. Even though the heat balance involving feedback to the gas path determines the dynamic characteristics at each time step, the gas dynamics is assumed to react infinitely fast. In essence, the time scale in gas-path kinetics is several orders of magnitude small relative to the time scale of thermal response of the refractory wall. Therefore, the gas temperatures are modelled as algebraic functions of other process variables (e.g. refractory wall temperatures) and the associated boundary conditions based on the principles of singular perturbation [**19**]. Finally, the slowest time scale, in which anomalies (i.e. deviations from the nominal condition due to incipient damage) are expected to evolve, may stretch to days of operation. This implies that refractory failures causing performance degradation occur on a time scale that is several orders of magnitude smaller than the gas-path kinetics and the thermal response of the refractory wall.

From the perspectives of degradation monitoring and slow-scale damage evolution, the following two time scales of operation are relevant:

1. Heat transfer through the composite wall at the fast time scale over which the time series data are collected.
2. Refractory wall degradation at the slow time scale over which maintenance decisions are made.

For example, assuming that the usual life span of the refractory wall ranges approximately from 4 to 14 months, it would be worthwhile to schedule one monitoring test every day or alternate days, and such a test of stimulus injection may last less than 5 min (see section 5.2 for a typical test example). In the sequel, the algorithm of degradation monitoring in refractory walls is validated on the computer simulation model of a generic entrained-bed slagging gasifier.

3.2 Gas-path kinetics model

The gas-path kinetics in the simulation test bed are built upon the steady-state model of Texaco Downflow Entrained-Bed Pilot Plant Gasifier, reported by Wen and Chuang [**2**]. While the details of the experimentally validated model equations are available in open literature, a compact description is provided in this section for the completeness of the paper. The present model of the gasifier uses coal liquefaction residues and coal–water slurries as feedstocks and simulates the steady-state responses of the plant under different operating conditions. The execution time of the simulation model is significantly small (e.g. in the order of seconds on a desktop computer) as compared to a conventional CFD model, which is essential from the perspectives of real-time degradation monitoring and decision-making in gasifier operations. Following Fig. 2, the entrained-bed gasifier is conceptually divided into three zones.

1. *Pyrolysis and volatile combustion zone*. The input slug (fuel + steam), when heated to high temperatures, decomposes and produces volatile materials that consist of a mixture of combustible gases (i.e. CO, H_2, and CH_4), carbon dioxide (CO_2), water vapour (H_2O), and tar. Since the pyrolysis zone is rich in oxygen, burning of combustible gases is assumed to be complete. A large amount of heat is thus released in the gas phase, which heats the solid fuel rapidly to the pyrolysis temperature.
2. *Combustion and gasification zone*. In this zone, the de-volatilized char reacts with the remaining oxygen to produce CO/CO_2 (char-oxygen reaction) and with steam (char-steam reaction) and CO_2

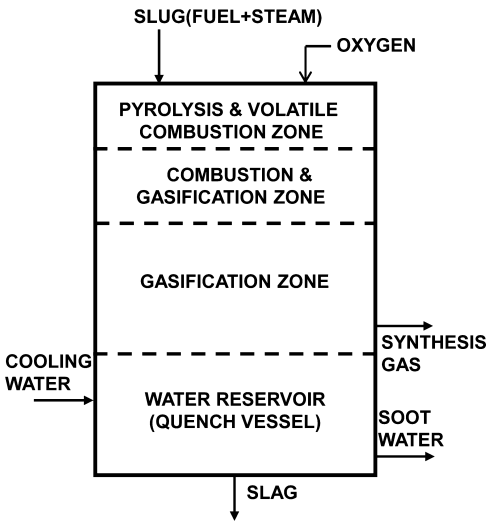

Fig. 2 Gas-path model schematic

(char-CO_2 reaction) to produce CO and H_2. The combustible gases, CO and H_2, in turn react in the gas phase with O_2 to further increase the heat generation.

3. *Gasification zone*. The combustion gas flows into this zone where heterogeneous reactions occur. In addition to the char-H_2O and char-CO_2 reactions, three very important reactions occur in this zone.
   (a) Synthesis gas ($CO + H_2$) is produced in a reversible reaction, which is known as the *water-gas-shift reaction*.
   (b) Methane (CH_4) is produced by hydro-gasification of char.
   (c) The methane-steam ($CH_4 + H_2O$) reforming reaction reduces methane to produce synthesis gas and hydrogen.

The final products leaving the gasifier are largely synthesis gas ($CO + H_2$) and CO_2. Since volatile materials are burned in the O_2-rich zones, no tar appears in the product; minor species of the gas product are H_2S and CH_4. Details of chemical kinetics in the above reactions are available in reference [**2**]. The reaction chamber, that is 3.44 m high, is divided into 119 compartments (of varying size and shape) from top to bottom for model formulation. The heat balance equation for a typical compartment is obtained as:

$$\mathfrak{h}^i_{\text{out}} - \mathfrak{h}^i_{\text{in}} = \mathfrak{h}^i_{\text{gen}} - q^i_{\text{loss}} \tag{1}$$

where $\mathfrak{h}^i_{\text{out}}$ is the total enthalpy output, $\mathfrak{h}^i_{\text{in}}$ the total enthalpy input, $\mathfrak{h}^i_{\text{gen}}$ the generated enthalpy, and q^i_{loss} the total heat loss through the reactor wall in the ith compartment.

The profiles of gas flow and solid-particle temperatures and material concentration along the reactor are obtained by solving the simultaneous algebraic equations of heat and mass balance for each compartment and by taking gasification kinetics, transport rates, and hydrodynamics of the gasifier into consideration. The gas phase is assumed to be completely mixed at the reactor entrance that is followed by a region approximating the plug flow. The solid phase is modelled as a plug-flow process throughout the reactor.

Execution of the simulation model is designed to be highly reliable over a wide range of operating conditions for different types of coal (e.g. Illinois No. 6 and Wyodak) [**2**]. The results (see section 5) of numerical simulation from the present model were compared with the experimental data for different input coal feed rates (ranging from 56 to 180 g/s) and different O_2–fuel ratio. The results were in very close agreement with the experimental data and the results reported by Wen and Chuang [**2**] at different operating conditions and different types of coal. Parametric sensitivity of the model was tested and optimum operating conditions were searched to provide a better understanding of the performance at various operating points.

3.3 Slag heat transfer and flow model

The gas-path kinetics model, developed in reference [**2**], assumed a thin-wall boundary condition to simulate the Texaco Down-flow Entrained-Bed Pilot Plant Gasifier. Due to lack of sufficient experimental data, the thermal condition for such a boundary wall was assumed to have a uniformly varying temperature distribution starting at 2100 K at the top of the gasifier and decreasing at the rate of 600 K/m. Even though this assumption succeeded in validating the experimental results to a reasonable accuracy, additional details, such as slag flow, and heat transfer through the refractory, are required to be incorporated in the simulation model for detection of incipient anomalies and the associated damage in the refractory walls. A change in the spatial-temporal characteristics of the composite wall temperature is considered to be an important clue for detecting the health status of the refractory lining (please refer section 2). The temperature variations across the cross-section of the gasifier lining at different vertical levels provide useful information for degradation monitoring.

The temperature characteristics in the refractory wall can be generated using the integrated model of heat transfer and slag flow. The refractory wall, illustrated in Fig. 3, is composed of three sections. The innermost layer in contact with the slag or the hot gasifier gases is made up of the heat-resistant refractory bricks. The outermost layer is the insulating asbestos-cement wall. A thin sheet of metal is sandwiched between the inner and outer layers. The material properties and physical parameters of the refractory wall are listed in Table 1.

The equations that describe the slag layer include the conservation equations of momentum, energy, and mass [**20**]. The heat transfer and mass-balance equations within the slag layer have been derived based on the studies conducted by Bockelie *et al.* [**21**] and Cundick *et al.* [**22**] and a final heat-balance has been performed between the gas-path and the combustor wall. The resulting equations are briefly presented below.

The major assumptions in modelling the transport phenomena inside the slag layer are listed below.

(a) representation of the slag as a Newtonian fluid;
(b) negligible inertial forces and pressure gradient.

The resulting equation of motion [**21**] is given as

$$\frac{\partial}{\partial r}\left(\mu \frac{\partial u}{\partial r}\right) = \rho g \tag{2}$$

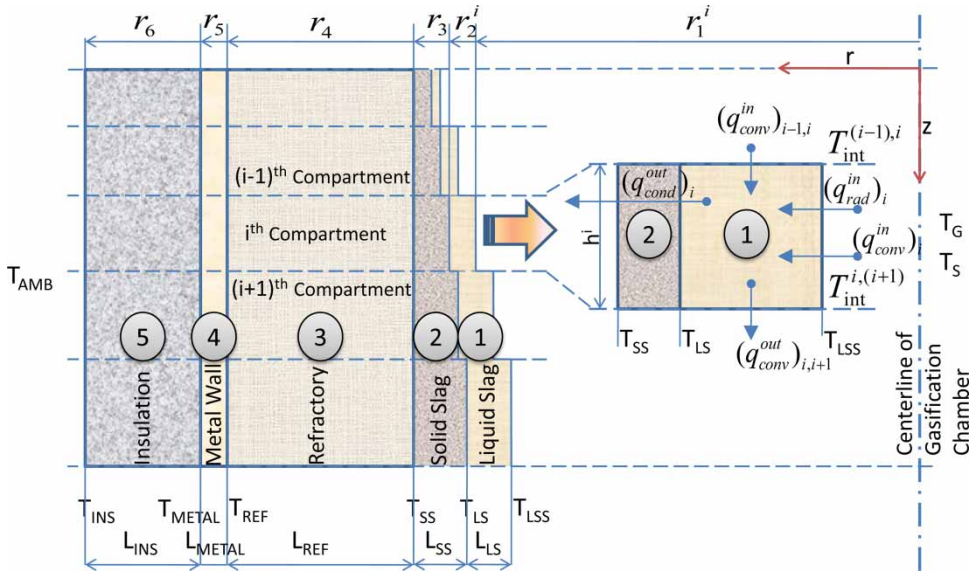

Fig. 3 Composite model of slag layer and refractory wall

Table 1 Physical dimensions and material properties of composite wall

Wall part	Material	Inner radius R_i (cm)	Conductivity W/(m K)	Specific heat J/(kg K)	Density (kg/m^3)	Emissivity, ϵ
Insulation	Asbestos-cement board	95	0.744	700	1050	0.96
Metal layer	Steel	92.5	46	472	7870	–
Refractory	Alumina-based	77.5	10	935	3000	–
Solid slag layer	–	Variable	$24.3 - 0.0416(T_{cv} - 273) + 1.81 \times 10^{-5}(T_{cv} - 273)^2$	1.382×10^3	2.5×10^3	–
Liquid slag layer	–	Variable	$24.3 - 0.0416(T_{LSS} - 273) + 1.81 \times 10^{-5}(T_{LSS} - 273)^2$	1.382×10^3	2.5×10^3	–

where μ is the slag viscosity, r is the distance in the radial direction, ρ is the slag density, and $u(r, z)$ is the velocity of the slag in the z-direction at a certain radius r from the gasifier axis.

The energy conservation equation has a more complicated structure than the above equation of motion because the conduction process carries the bulk of thermal energy from the hot gases in the gasifier radially outward to the cool ambient, while the vertical flow of heat is ascribed to slag movement. Solution of this energy transport problem in its entirety calls for a two-dimensional numerical model that would be computation-intensive for real-time analysis on a commercially available inexpensive platform (e.g. a desktop computer). To circumvent this problem, heat transfer through the refractory materials is assumed to be entirely due to conduction, i.e. the effects of convection and viscous dissipation are assumed to be relatively insignificant. Consequently, heat transfer through the slag has been modelled as a one-dimensional problem [**21**, **22**] and the convective term only appears in the final heat balance. Based on this assumption, the heat-flow equation is derived as

$$q = -k\frac{\partial T}{\partial r} \tag{3}$$

where $q(r, z)$ is the heat flux normal to the slag layer due to conduction, $T(r, z)$ the slag temperature, and k the thermal conductivity of the slag.

The numerical solution of the above equations is obtained by transforming the governing equations with respect to the independent variables in the rz coordinate system to the zT coordinate system [**21**]. The transformed equations are listed as follows

$$\frac{\partial r}{\partial T} = -\frac{k}{q(z, T)} \tag{4}$$

$$\frac{\partial u}{\partial T} = \frac{k\tau}{\mu q(z, T)} \tag{5}$$

$$\frac{\partial q}{\partial T} = 0 \tag{6}$$

where $\tau = \mu \partial u/\partial r$ is the shear force. The viscosity μ of the liquid slag is given by the Weymann relation [**20**] as

$$\mu(T) = AT\mathrm{e}^{B/T} \quad \text{for} \quad T > T_{cv} \tag{7}$$

where A and B are constants, and T_{cv} is the critical value of temperature below which the fluid slag transforms into a Bingham plastic state [**21**]. In other words, T_{cv} is the highest temperature at which solid and liquid

Table 2 Model parameter values

Parameter	Value	Parameter	Value
A	8.5382×10^{-12}	C	1800 K
B	3.6281×10^{4}	g	$9.8\,\mathrm{m/s^2}$
ρ	$2.5 \times 10^{3}\,\mathrm{kg/m^3}$	U_0	$1.43 \times 10^{3}\,\mathrm{W/m^2\,K}$
T_{cv}	1400 K	T_{AMB}	298 K
K	10		

slag can co-exist. The values of critical parameters such as A, B, and T_{cv} are listed in Table 2.

Finally, the equation for conservation of mass is given by

$$\dot{M}_{\mathrm{s}}^{i} = \int_{r_1^i}^{r_2^i} \rho u^i \,\mathrm{d}r \tag{8}$$

where the superscript i indicates the ith compartment, $\dot{M}_{\mathrm{s}}^{i}$ the mass flux, $u^i(r,z)$ the slag velocity in z-direction, and r_1^i and r_2^i indicate the inner and outer radius of liquid slag, respectively.

Under a steady-state condition, the mass flux of slag out of a compartment is equal to the fly-ash deposition rate in the same compartment, which depends on several factors including the type of ash, the nature of the refractory surface, the temperature of the hot ash particles, and the velocity with which the particles impinge upon the refractory surface. The amount of entrained ash in the slag flow [**23**] is given by

$$\dot{M}_{\mathrm{s}}^{i} = K\,\mathrm{Ash}_{\mathrm{tot}} h_i \left(\frac{C - T_{\mathrm{S}}^{i}}{T_{\mathrm{S}}^{i}} \right) \tag{9}$$

where K and C are correlation constants that are determined from experiments (Table 2), $\mathrm{Ash}_{\mathrm{tot}}$ the total ash efflux at the gasifier exit, h_i the height of the ith compartment, and T_S the solid ash particle temperature in the combustor chamber.

By combining equations (4) to (7), the velocity profile at the liquid slag layer in the ith compartment is derived as

$$u^i(T) = \rho g \left(\frac{k}{(q_{\mathrm{cond}}^{\mathrm{out}})_i} \right)^2 \int_{T_{\mathrm{LS}}^i}^{T} \frac{T_{\mathrm{LSS}}^i - \theta}{\mu(\theta)} \,\mathrm{d}\theta \tag{10}$$

where $(q_{\mathrm{cond}}^{\mathrm{out}})_i$ is the heat flux emanating normally outward from the ith compartment through the slag layer as shown in the inset in Fig. 3. The mass flux $\dot{M}_{\mathrm{s}}^{i}$ in the ith compartment is obtained from equations (8) and (4) as

$$\dot{M}_{\mathrm{s}}^{i} = \frac{\rho k}{(q_{\mathrm{cond}}^{\mathrm{out}})_i} \int_{T_{\mathrm{LS}}^i}^{T_{\mathrm{LSS}}^i} u_i(\theta) \mathrm{d}\theta \tag{11}$$

A combination of equations (11) and (10) yields

$$\dot{M}_{\mathrm{s}}^{i} = \frac{\rho k}{(q_{\mathrm{cond}}^{\mathrm{out}})^i} \times \int_{T_{\mathrm{LS}}^i}^{T_{\mathrm{LSS}}^i} \left[\rho g \left(\frac{k}{(q_{\mathrm{cond}}^{\mathrm{out}})_i} \right)^2 \int_{T_{\mathrm{LS}}^i}^{T} \frac{T_{\mathrm{LSS}}^i - \theta}{A\theta \mathrm{e}^{B/\theta}} \mathrm{d}\theta \right] \mathrm{d}T \tag{12}$$

where $\dot{M}_{\mathrm{s}}^{i}$ on the left-hand side of equation (12) is evaluated from equation (9). The preceding derivations are based on the assumption of quasi-steady thermal transport by neglecting the conjugate heat transfer (i.e. heat conduction and convection in the transverse direction). As shown in Fig. 3, heat balance in the slag layer for the ith compartment yields the steady-state energy equation in the following form

$$(q_{\mathrm{conv}}^{\mathrm{in}})_{i-1,i} + (q_{\mathrm{conv}}^{\mathrm{in}})_i + (q_{\mathrm{rad}}^{\mathrm{in}})_i = (q_{\mathrm{conv}}^{\mathrm{out}})_{i,i+1} + (q_{\mathrm{cond}}^{\mathrm{out}})_i \tag{13}$$

where $(q_{\mathrm{conv}}^{\mathrm{in}})_{i-1,i} \equiv \dot{M}_{\mathrm{s}}^{(i-1),i} \mathrm{Cp}(T_{\mathrm{int}}^{(i-1),i}) T_{\mathrm{int}}^{(i-1),i}$ is convective heat influx as a result of slag flow from upper chamber; $(q_{\mathrm{conv}}^{\mathrm{in}})_i \equiv \dot{M}_{\mathrm{s}}^{i} \mathrm{Cp}(T_S^i) T_S^i$ is convective heat influx as a result of deposition of flyash into the already existing liquid slag layer; $(q_{\mathrm{rad}}^{\mathrm{in}})_i \equiv U_0 A^i (T_{\mathrm{G}}^i - T_{\mathrm{LSS}}^i)$ is radiative heat flux from the hot gases in the combustion chamber; $(q_{\mathrm{conv}}^{\mathrm{out}})_{i,i+1} \equiv \dot{M}_{\mathrm{s}}^{i,(i+1)} \mathrm{Cp}(T_{\mathrm{int}}^{i,(i+1)}) T_{\mathrm{int}}^{i,(i+1)}$ is convective heat outflux as a result of slag flow into the lower chamber; and $(q_{\mathrm{cond}}^{\mathrm{out}})_i$ is conductive heat outflux through the refractory wall.

The algorithm of the integrated model of the gasification system is presented in section 3.5 after the description of refractory heat transfer model.

3.4 Refractory heat transfer model

The elements of the composite wall and the solid and liquid phases of the slag are marked by numerics $1, 2, \ldots, 5$ for ease of nomenclature starting from the inside of the gasification chamber (Fig. 3). The conductivity of the jth segment is denoted by k_j, i.e. $k(r) = k_j$ for $r_j \leqslant r \leqslant r_{j+1}$. The conductive heat outflux $(q_{\mathrm{cond}}^{\mathrm{out}})_i$ through the refractory from the ith compartment is used to calculate the temperature profile in each section of the composite refractory wall as well as the widths of solid and liquid slag deposits. The steady-state heat conduction equation is given as

$$(q_{\mathrm{cond}}^{\mathrm{out}})_i = \frac{-2\pi k_j (T^i(r_j) - T^i(r_{j+1}))}{\ln(r_j / r_{j+1})} \tag{14}$$

where r_j (for $j = 1, \ldots, 5$) is the radial distance to the beginning of the surface of the jth segment in the slag-refractory wall (Fig. 3) and $T^i(r)$ denotes the temperature in the ith compartment at a certain radius r. The radiative heat transfer for the outer surface of the insulator is given as

$$(q_{\mathrm{cond}}^{\mathrm{out}})_i = \epsilon \sigma h_i (T^i(r_6)^4 - T_{\mathrm{AMB}}^4) \tag{15}$$

The calculation of temperatures at successive radii is dependent on the fact that the liquid and solid slag layer thicknesses are variable. The presence of solid slag layer depends on whether the temperature T_{SS} is lower than the critical melting point temperature T_{cv}.

3.5 Description of the algorithm

This section presents the algorithm that integrates the individual models of gas-path kinetics, slag flow, and heat transfer through the slag-refractory composite structure. The algorithm is described below.

1 Initialization: Provide an initial guess for T^i_{LSS};
Result: T^i_{LS}, T^i_{SS}, T^i_{REF}, T^i_{METAL}, T^i_{INS}, L^i_{LS}, L^i_{SS}, $(q^{\mathrm{out}}_{\mathrm{cond}})_i$
2 **while** T^i_{LS} *has not converged* **do**
3 Assume $T^i_{\mathrm{LS}} = T_{\mathrm{cv}}$;
4 Evaluate $(q^{\mathrm{out}}_{\mathrm{cond}})_i$ from Eqn. (12);
5 Knowing T_{AMB}, $(q^{\mathrm{out}}_{\mathrm{cond}})_i$, and the refractory wall properties, calculate T^i_{SS}, T^i_{REF}, T^i_{METAL}, T^i_{INS} using the steady-state heat conduction and radiation Eqs. (14) and (15), respectively;
6 **if** $T^i_{\mathrm{SS}} < T_{\mathrm{cv}}$ **then**
7 Solid slag layer exists;
8 Calculate L^i_{SS} and L^i_{LS} using steady state heat conduction Eq. (14);
9 exit;
10 **else**
11 Assumption $T^i_{\mathrm{LS}} = T_{\mathrm{cv}}$ is wrong;
12 Update $T^i_{\mathrm{LS}} = (T_{\mathrm{cv}} + T^i_{\mathrm{LSS}})/2$;
13 **if** $T^i_{\mathrm{LS}} = T^i_{\mathrm{SS}}$ **then**
14 Calculate L^i_{LS} and EXIT;
15 **else**
16 GO TO STEP 4
17 **end**
18 **end**
19 **end**
20 Calculate $T^{i-1,i}_{\mathrm{INT}} = (T^{i-1}_{\mathrm{LSS}} + T^{i-1}_{\mathrm{LS}})/2$ and $T^{i,i+1}_{\mathrm{INT}} = (T^i_{\mathrm{LSS}} + T^i_{\mathrm{LS}})/2$;
21 Update T^i_{LSS} from heat balance Eqn. (13);
22 **if** T^i_{LSS} *does not match previous value within a threshold* **then**
23 GO TO STEP 2
24 **else**
25 EXIT
26 **end**
27 Pass T^i_{LSS} to gas-path model and update T^i_{G} by Wegstein root search method [**2**];
28 **if** T^i_{G} *matches previous value within a threshold* **then**
29 EXIT
30 **else**
31 GO TO 21
32 **end**

The algorithm involves multiple iterations to evaluate all the interface temperatures at different segments of the slag-refractory composite structure and also the thicknesses of solid and liquid slag layers at different cross-sections along the vertical axis of the gasification system.

4 DEGRADATION MONITORING OF THE REFRACTORY

The refractory damage monitoring procedure is envisioned as a combination of data-driven and model-based techniques. As described in the previous section, the simulation model generates a steady-state spatial distribution of temperature profile that should be routinely calibrated with the observed readings of the sensor array under the nominal (i.e. healthy) conditions. In the event of anomalous (i.e. damage evolution in the refractory) conditions, the refractory temperature profile measured by sensor readings deviates from the one derived from the simulation model that operates at the nominal condition.

This refractory degradation monitoring system utilizes both model-based and sensory information, where the model generates the temperature profile at the nominal (i.e. healthy) condition under (possibly) different operating points, and the sensors provide measurements of temperature at different locations under (possibly) different anomalous conditions. Therefore, a comparison of model and sensor responses provides an indication of anomalies, i.e. departure of the gasification system from its nominal condition. However, upon progression of damage in the refractory wall, the difference between the steady-state temperature profiles generated from the observed sensor data and the simulation model may not necessarily provide a sufficient index of anomalies due to a multitude of factors. For example, inaccurate model predictions may result from inherent uncertainties in the gasification plant and unavoidable disturbances in the operating environment. A possible consequence is perturbation in the steady-state profile of the computed refractory wall temperature, which may give rise to false alarms and missed detections except possibly for very large faults. Furthermore, if the gasification system is operated under steady-state conditions, the time-series data of refractory wall temperature T_{REF} generated from the sensor array may not be sufficiently rich in information, because variations in the usual load demand may not be an appreciable stimulus to the damage detection system due to the presence of a large thermal mass and capacitance that acts as a low-pass filter and smooths out the effects of demand fluctuations.

In view of the above possible situations, a viable alternative is to artificially inject stimuli into the gasifier system in the form of small-amplitude fluctuations in the coal-feed rate. Such induced fluctuations in the coal-feed rate would be merely a maintenance procedure to be carried out solely for the degradation monitoring tests and last for at most a few minutes only when these tests are conducted. The purpose of this excitation is to monitor the response of the system under an external stimulus that generates the dynamic temperature response T_{REF}. Such tests will not have any bearing on the performance of the gas production process. The decision for scheduling of the proposed degradation monitoring procedure is largely dependent on the time scales in which the gasification plant operates. Therefore, rather than using the steady-state profiles in conjunction with simple (e.g.

threshold-based detection) techniques, this paper has used the dynamic response of the system generated by an external excitation of cyclically varying coal-feed rate. The excitation must be sufficiently large enough to amplify the effects of the anomalies while the effects of environmental disturbances and other uncertainties stay the same. This technique is similar to the one adopted by a medical doctor who deliberately injects a certain medication into the patient and observes the response, which could be significantly different for a healthy and a sick person, thereby enabling diagnosis of the illness.

A slag-refractory heat transfer model is developed to obtain the dynamic heat transfer characteristics at different segments of the composite wall (Fig. 3). The refractory heat transfer response is generated for cyclic step changes in the input coal-feed rate from one steady state to another. Following the nomenclature described in section 3.4, $T^i(r,t)$ denotes the temperature in the ith compartment as a function of the radius r at time t. The conductivity and diffusivity of the jth segment in the finite-difference scheme are denoted by k_j and α_j, respectively.

The governing equations for heat transfer through the composite wall are

$$\frac{\partial T^i(r,t)}{\partial t} = \frac{1}{r}\frac{\partial}{\partial r}\left(\frac{\alpha_j}{r}\frac{\partial T^i(r,t)}{\partial r}\right) \quad \text{at } r_j^i < r < r_{j+1}^i, \quad j = 1,\ldots,5 \tag{16}$$

The associated boundary conditions at the ith compartment are:

$$\begin{aligned}
&-k_1\frac{\partial T^i(r,t)}{\partial r} = U_0(T_G^i - T^i(r,t)) + \dot{M}_s^i \mathrm{Cp} T_s \quad \text{at } r = r_1^i \\
&-k_5\frac{\partial T^i(r,t)}{\partial r} = \epsilon\sigma(T^i(r,t)^4 - T_{\mathrm{AMB}}^4) \quad \text{at } r = r_6^i \\
&T^i(r)|_{(r_j^i)^-} = T^i(r)|_{(r_j^i)^+} \quad \text{for } j = 2,\ldots,5 \\
&-k_j\left.\frac{\partial T^i(r,t)}{\partial r}\right|_{(r_j^i)^-} = -k_{j+1}\left.\frac{\partial T^i(r,t)}{\partial r}\right|_{(r_j^i)^+} \quad \text{for } j = 2,\ldots,5
\end{aligned} \tag{17}$$

and the initial condition at the ith compartment is:

$$T^i(r,t)|_{t=0} = T_0^i(r) \quad \text{at } r_j^i < r < r_{j+1}^i, \ j = 1,\ldots,5 \tag{18}$$

The above system of equations is solved with an explicit finite-difference scheme. For each compartment, it is assumed that the gas temperature T_G^i reacts to any disturbances infinitely fast and immediately attains a new steady-state value as a consequence of singular perturbation analysis [**19**].

As described earlier in section 3.1, from the perspectives of degradation monitoring and the associated concept of fast-scale time-series data and slow-scale damage evolution, the following time scales of operation are relevant.

1. Heat transfer through the composite wall at the fast time scale over which the time-series data are collected.
2. Refractory wall degradation at the slow time scale over which maintenance decisions are made.

For example, assuming that the usual life span of the refractory wall ranges approximately from 4 to 14 months, it would be worthwhile to schedule one monitoring test every day or alternate days, and such a test of stimulus injection may last for a few minutes. In the present study, the stimulus to the gasification plant is provided by cyclically fluctuating the coal-feed rate using step changes from 60 to 100 g/s, and vice versa, with one cycle lasting for 2.5 min. In this manner, the time-series data of the dynamic response of temperature T_{REF} is generated.

Once the dynamic response of the system is generated in terms of time-series data, an analytical tool is needed for anomaly detection using advanced signal processing and pattern identification. This paper has adopted a recently reported robust pattern identification method, called SDF [**4**, **8**, **24**], that analyses (statistically stationary) time-series data generated from the dynamic response of refractory temperature (T_{REF}) for real-time degradation monitoring of the refractory wall. Recent literature has reported experimental validation and efficacy of SDF in terms of early detection of anomalies and robustness to measurement noise in several different applications, such as fatigue damage monitoring in structural materials [**9**, **10**, **25**] and fault detection in active electronic circuits [**11**, **12**]. (Please see Appendix 2 for details of SDF.)

The time-series data of the dynamic response of temperature T_{REF} is analysed using SDF to generate the statistical patterns of damage evolution (for details please refer section 5.2). The time-series data, generated by the sensor array, are statistically quasi-stationary in the time scale of the heat-flow process dynamics in the refractory wall. However, as damage progresses on the slow scale, these statistical patterns deviate from the nominal condition and provide an indication of the evolving damage.

The next important consideration is placement of the temperature sensors around the refractory wall on its outer (cylindrical) surface. A sensor placement configuration is illustrated in Fig. 4, where all sensors are placed symmetrically around the circumference equidistant from each other both in the axial and circumferential directions; however, optimal placement of sensors is a topic of future research.

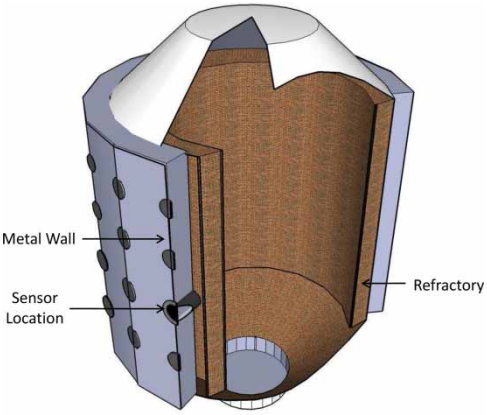

Fig. 4 Schematic diagram of sensor placement on gasifier wall

Sensor placement on the outer surface of the refractory wall not only protects the sensors from temperature extremes and corrosion in the gasifier chamber, but also makes sensor installation, maintenance, and repair much easier. A properly designed hole drilled through the insulation and metal wall should be able to house thermocouples or any other temperature sensor without any adverse effects on the gasifier operation. The model employed in this paper is two-dimensional, whereas the heat transfer, damage, and slag flow involve three coordinates of r, θ, and z. However, in the nominal condition, this is not considered to be a constraint because circumferential symmetry of the gasification chamber ensures that the two-dimensional model represents operations of the three-dimensional plant. Once the refractory has been damaged, this circumferential symmetry might be lost. In that case, a comparison of the true sensor readings and the readings predicted by the two-dimensional nominal model would be an indication of the anomaly in the gasification system.

5 SIMULATION RESULTS AND DISCUSSION

A brief description of the simulation model of an integrated gasification system including the heat transfer characteristics through the composite structure of the refractory and the slag has been provided in section 3. The steady-state response of the gasification system is generated from this simulation model that describes the gas-path kinetics, slag flow, and the slag-refractory heat transfer phenomena. The dynamic characteristics of the refractory wall temperature (T_{REF}) are generated for the purpose of degradation monitoring and maintenance (see section 4) by providing an external excitation of cyclically varying coal-feed rate. The simulation model of the entrained-bed slagging gasification system, in its entirety, is capable of tracking the performance of the gasification system under both steady-state and dynamic operations, and provides the steady-state and dynamic temperature profile at all cross-sections in the refractory wall.

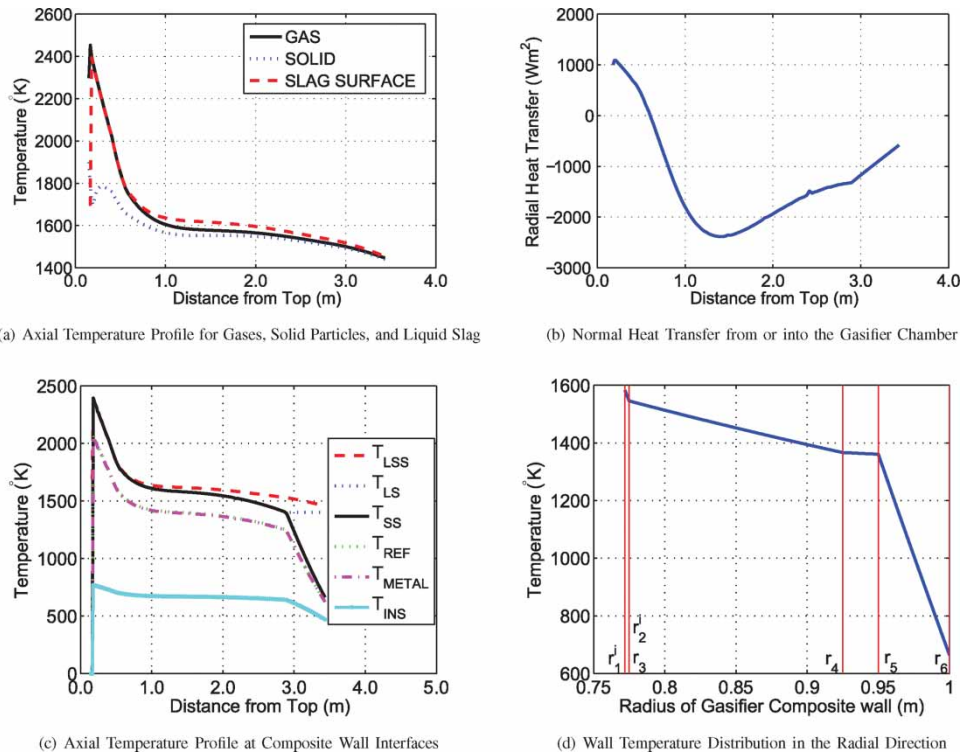

(a) Axial Temperature Profile for Gases, Solid Particles, and Liquid Slag

(b) Normal Heat Transfer from or into the Gasifier Chamber

(c) Axial Temperature Profile at Composite Wall Interfaces

(d) Wall Temperature Distribution in the Radial Direction

Fig. 5 Steady-state distribution of gas temperature, wall temperature, and heat flux

5.1 Steady-state response of the gasification system

This section presents the results pertaining to steady-state response of the integrated simulation model of the gasification system described in section 3. Figure 5(a) shows the steady-state temperature profile in the axial direction for combustor gases, solid coal particles, and liquid slag surface. In the combustion zone, due to exothermic reactions, the gas temperature rises quickly, and a part of this thermal energy is transferred into the molten slag. In the later phase of gasification, the reactions are mostly endothermic and a part of the thermal energy carried by the molten slag is released back into the gasification chamber. Notably, there exists a point beyond which the gas temperature drops below the slag surface temperature. Consequently, the heat flux in and out of the gasification chamber changes direction, as seen in Fig. 5(b). The steady-state temperature profiles recorded at all interfaces in the composite wall are shown in Fig. 5(c). A large temperature difference occurs across the insulator, and its outer surface approximately remains at a uniform temperature from top to bottom of the gasifier. Figure 5(d) shows the steady-state temperature profile across the composite wall at a typical axial location. The temperature sensors are installed at the outer surface of the refractory at a radius of 0.925 m, depicted as r_4 in Fig. 5(d).

5.2 Dynamic response for degradation monitoring

This subsection presents the results pertaining to dynamic response of the integrated simulation model of the gasification system for degradation monitoring (see section 4) of the refractory wall. The time-series response of the refractory wall temperature (T_{REF}) is generated by providing an external excitation of cyclically varying coal-feed rate.

5.2.1 Numerical simulation and data acquisition

To generate the dynamic response of refractory wall temperature, the coal-feed rate is cyclically varied as step changes between 60 and 100 g/s with each cycle lasting for 2.5 min. Figure 6 exhibits the step response of a typical temperature sensor for the above excitation under the nominal condition. Time-series data of the refractory wall temperature (T_{REF}) is generated from the simulation model under the above excitation for the nominal (i.e. healthy) condition. Subsequently, in order to generate the time-series data for different anomalous conditions of the refractory wall, information of the degraded wall geometry is injected into the simulation model. It is assumed that the effects of refractory damage lead to a reduction in the wall thickness and, consequently, an increase in the inner radius

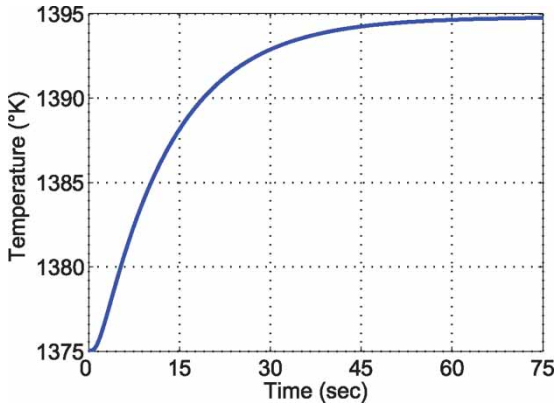

Fig. 6 Slag temperature dynamic response of the gasifier

of the wall at different locations. Therefore, reduction in refractory wall thickness is taken as an independent variable that can be mapped to the progression of time in the slow time scale in a gasification system for the purpose of damage monitoring; such a map would be dependent on the operating conditions and type of the gasifier. The refractory wall damage can be randomly injected at any axial location of the gasification system. In the present study, damage is incrementally injected into the simulation model at a randomly chosen gasifier compartment 60 (see section 3), which is approximately located in the middle of the gasifier. The refractory wall thickness is depleted by 1 mm each time and simulation is run under above-mentioned excitation to generate the time-series data of dynamic response of refractory temperature (T_{REF}). In the test runs, time-series data are collected for each damaged condition in increments of 1 mm until the refractory wall thickness in the simulation model is reduced by 10 mm, which typically corresponds to a single spalling event [**13**].

5.2.2 Data analysis

Time-series data for both nominal and anomalous conditions have been analysed using SDF (see Appendix 2) for generation of statistical patterns of evolving anomalies. For symbol sequence generation, wavelet-based maximum entropy partitioning has been used with the gaus2 (i.e. Mexican Hat) basis function; the symbol alphabet size for partitioning is chosen to be $|\Sigma| = 15$ and the depth $D = 1$ for construction of the finite-state machine. Hence, the number of states in the finite-state machine is $n = |\Sigma|^D = 15$. Details of SDF are available in Appendix 2 and references cited therein.

Figure 7 shows the results of SDF-based analysis of the time-series data sets. The top row of Fig. 7 shows the time-series data sets of refractory temperature for three different damage conditions of the refractory:

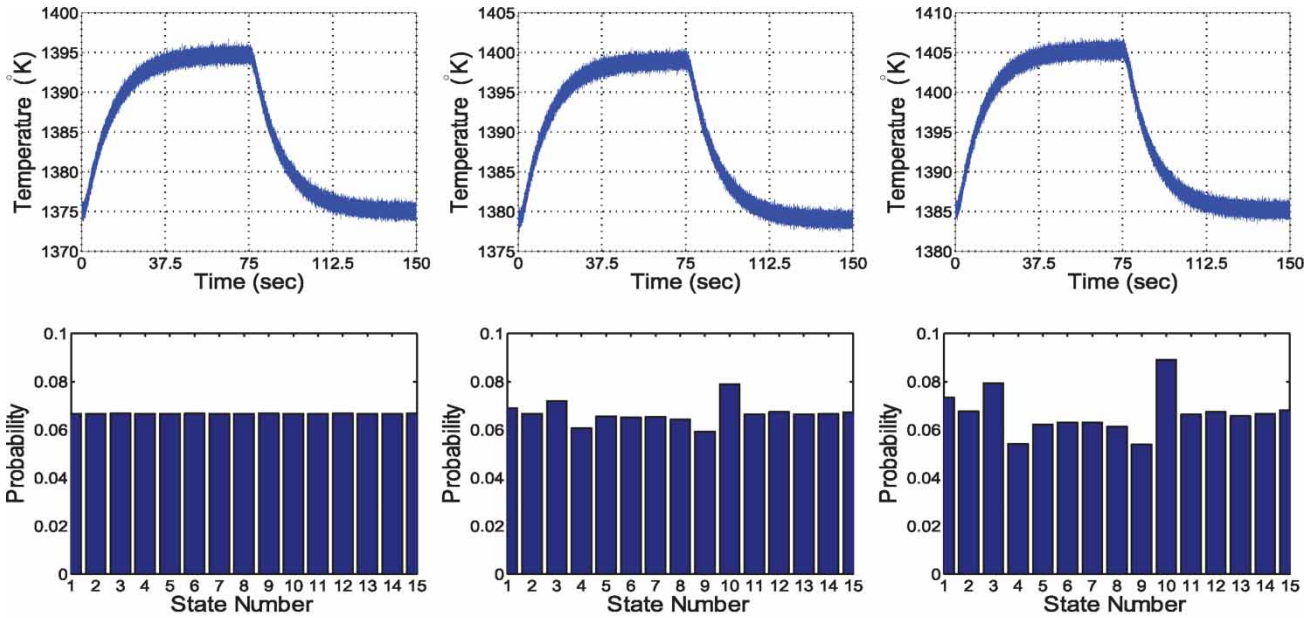

Fig. 7 Evolution of statistical patterns with refractory wall degradation

(a) nominal (i.e. healthy) condition, (b) 5 mm refractory damage, and (c) 10 mm refractory damage that corresponds to a typical spalling event. The time-series data are recorded for a compartment in the middle of the refractory (i.e. compartment 60), where the damage is injected. Each plot in the top row of Fig. 7 shows the time-series data of refractory temperature generated from a single cycle of excitation in the coal-feed rate. The set of test data comprises of a sufficiently large number of excitation cycles to generate statistically rich data; sufficiency of data length is governed by a stopping rule that has been presented in earlier publications [**8**, **26**]. The time-series data sets have been injected with multiplicative noise to closely represent real-time experimental data that are commonly contaminated with measurement and process noise. The noise-contaminated signal is obtained by $\tilde{S} = S(1 + \eta)$, where S and $\tilde{S}$ are the uncontaminated and the noise-contaminated signals, respectively, and η is zero mean Gaussian noise with SD 0.002. This noise generates fluctuations in temperature readings with a SD of ≈ 2 K. The bottom row of Fig. 7 shows the histograms of probability distribution that are generated from SDF analysis of corresponding time-series data sets. The histograms represent the statistical patterns of damage evolution at the above three different damage conditions. As a consequence of maximum entropy partitioning [**7**] (see also Appendix 2) at the nominal condition, the probability distribution is uniform as seen in plot (a) of Fig. 7. As damage evolves, the statistical patterns gradually deviate from the nominal pattern of uniform distribution as seen in plots (a), (b), and (c) of Fig. 7.

Figure 8 shows the profile of anomaly measure with gradual evolution of damage in the refractory wall. Anomaly measure is quantitatively expressed as a (scalar) distance between the statistical patterns (i.e. probability distributions) corresponding to an anomalous condition and the nominal condition, which are generated using SDF of time-series data. The distance function is chosen to be the Euclidean norm of the difference between the two patterns (see equation (21) in Appendix 2). A non-zero value of anomaly measure indicates deviation from the nominal condition and therefore provides a warning of incipient damage. It is seen in Fig. 8 that the anomaly measure profile grows as the damage progresses in the refractory wall. The SDF algorithms in this paper are implemented on the

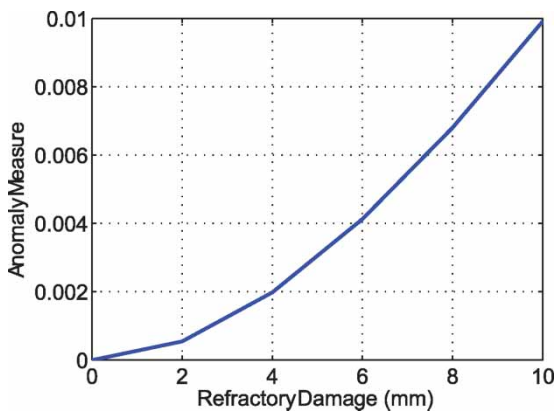

Fig. 8 Evolution of anomaly measure with refractory damage

MATLAB platform and are interfaced with the gasification plant simulation model for real-time degradation monitoring of the refractory wall.

Extensive numerical simulations have been conducted to test the validity of refractory damage monitoring algorithms. Time-series data sets were generated for several different compartments when the damage was injected at a particular location. The simulation results reveal the scenarios of damage monitored by sensors that are placed away from the location of fault (i.e. not in the immediate vicinity). This investigation has demonstrated that all sensors are able to capture the fault occurring at any location in the refractory. This is evident due to strong coupling inside the gasifier that rapidly adjusts to damaged refractory geometries to obtain new equilibrium conditions. Another observation indicates that sensors downstream are, in general, more or at least equally sensitive to the refractory faults upstream. The rationale for this observation is that the thermo-fluid coupling between the gas dynamics and the refractory surface due to prevalent downward flow of gas and slag produces a greater effect further downstream [**2**, **22**]. Evidently, this phenomenon makes fault localization and estimation [**9**] a difficult task because of possible non-unique solutions. However, all sensors have been successfully able to detect the growth of evolving anomalies in the refractory wall. Fault localization and estimation using information fusion from distributed sensors is an area of active research and has not been addressed in this paper. The above problems are also closely related to optimal sensor placement that is a topic of future research.

6 SUMMARY, CONCLUSIONS, AND FUTURE RESEARCH

This section summarizes the paper with pertinent conclusions. Areas of future research are recommended to overcome the limitations and shortcomings of the current work.

6.1 Summary

This paper addresses degradation monitoring of the refractory wall in coal gasification systems. The proposed algorithm of degradation monitoring is both model-based and data-driven and is built upon statistical pattern identification from sensor information in combination with an integrated simulation model of the gasification system. The initial part of the paper is a precursor to obtaining the dynamic response of pertinent plant variables to step changes in the coal feed rate, and involves modelling of individual subcomponents of the gasifier in lieu of the actual sensor information from an operating plant. To this end, the gas-path kinetics and the slag-refractory heat transfer characteristics have been modelled for computer simulation. These submodels have been integrated and the integrated model yields not only the cross-sectional steady-state spatial temperature profile, but also the dynamic response of the temperature sensors installed at different axial points in the composite wall of the gasifier wall under nominal operating conditions. In the later part of the paper, the dynamic response, rich in statistical information, is analysed with a pattern analysis tool, based on SDF [**4**], for real-time degradation monitoring of the refractory wall. The SDF algorithms have been implemented on a MATLAB platform and are interfaced with the gasification plant simulation model for emulation of real-time degradation monitoring.

6.2 Pertinent conclusions

The modelling and analysis efforts, presented in this paper, evince that SDF is a potentially viable tool for real-time degradation monitoring of the refractory wall in entrained-bed gasifiers. Specifically, the results of numerical simulation show that degradation monitoring and real-time prediction of evolving faults in the refractory wall are feasible under different load conditions of the gasification system by:

1. Installation of temperature sensors at appropriate locations on the outer surface of the refractory wall.
2. Statistical pattern (i.e. SDF) analysis of sensor time-series data in combination with the integrated simulation model for damage detection and failure prediction.
3. Incorporation of the ensemble of sensors, SDF algorithm of pattern analysis, and the integrated simulation model within the Instrumentation & Control system software and hardware.

The results of numerical simulation indicate that it might be possible to detect reduction in wall thickness of the order of a few millimetres. However, localization of wall degradation has not yet been addressed in the proposed method of degradation monitoring. It is envisioned that a combination of the temperature sensor array and a lumped-parameter model (that is executable on inexpensive platforms in real time) may serve as an instrumentation for localization of a degradation site in the circumferential direction of the gasifier wall; however, localization in the axial direction may not be straight-forward because of turbulent mixing of gases, changes in the chemical reaction types (e.g. exothermic and endothermic) in different sections of the gasifier, and downward flow of the molten slag. From this perspective, changes in the spatial distribution of refractory wall temperature as

outputs of the sensor array need to be investigated for localizing wall degradation in the axial direction. Further theoretical, computational, and experimental research is necessary before a combination of the real-time simulation model, sensor array, and the SDF-based degradation monitoring tool can be considered for incorporation into the Instrumentation & Control system of a commercial-scale gasification plant.

6.3 Recommendations for future research

Some of the topics of future research for life extension of refractory wall in gasification systems are delineated below.

1. Localization of wall degradation in both circumferential and axial directions by taking advantage of spatial distribution of refractory wall temperature as outputs of the sensor array.
2. Extension of the two-dimensional (i.e. r, z) heat-flow model of the refractory wall to a three-dimensional (i.e. r, θ, z) model to enhance the capabilities of detection and localization of simultaneous degradation at multiple locations in the refractory wall.
3. Quality assurance and automated calibration of sensor time-series data to circumvent incorrect estimates of damage and hence incorrect decisions for plant operation and maintenance.
4. The inverse problem for prediction of the remaining life of a gasifier through inspection of estimated damage measures at different epochs in the slow time scale for the refractory wall at hand.
5. Algorithm development for optimal placement of sensors on the refractory wall of a gasifier.

ACKNOWLEDGEMENTS

This work has been supported in part by the US Department of Energy under Battelle – Idaho National Laboratory Contract No. 00064349.

REFERENCES

1 **Clayton, S. J., Stiegel, G. J.,** and **Wimer, J. G.** Gasification markets and technologies – present and future. US DOE/FE report DOE/FE-0447, Department of Energy, 2002.

2 **Wen, C. Y.** and **Chuang, T. Z.** Entrained-bed coal gasification modelling. Interim Report submitted to Department of Energy (FE2274T1) West Virginia University, Morgantown, WV, USA, 1978.

3 **Dogan, C. P., Kwong, K. S., Bennett, J. P., Chinn, R. E.,** and **Dahlin, C. L.** New developments in gasifier refractories. San Francisco, California, USA; 2002, available from http://www.gasification.org/Docs/Conferences/2002/GTC02042.pdf.

4 **Ray, A.** Symbolic dynamic analysis of complex systems for anomaly detection. *Signal process*, 2004, **84**(7), 1115–1130.

5 **Duda, R. O., Hart, P. E.,** and **Stork, D. G.** *Pattern classification*, 2001, John Wiley, New York, NY, USA.

6 **Grondel, S., Delebarre, C., Assaad, J., Dupuis, J. P.,** and **Reithler, L.** A fatigue crack monitoring of riveted aluminium strap joints by lamb wave analysis and acoustic emission measurement techniques. *NDT & E Int.*, 2006, **35**, 339–351.

7 **Rajagopalan, V.** and **Ray, A.** Symbolic time series analysis via wavelet-based partitioning. *Signal Process*, 2006, **86**(11), 3309–3320.

8 **Gupta, S.** and **Ray, A.** Symbolic dynamic filtering for data-driven pattern recognition. Chapter 2 in pattern recognition: theory and application, (Ed. E. A. Zoeller), 2007 (Nova Science Publisher, Hauppage, NY, USA).

9 **Gupta, S.** and **Ray, A.** Real-time fatigue life estimation in mechanical systems. *Meas. Sci. Technol.*, 2007, **18**(7), 1947–1957.

10 **Gupta, S., Ray, A.,** and **Keller, E.** Symbolic time series analysis of ultrasonic data for early detection of fatigue damage. *Mech. Syst. Signal Process.*, 2007, **21**(2), 866–884.

11 **Chin, S., Ray, A.,** and **Rajagopalan, V.** Symbolic time series analysis for anomaly detection: a comparative evaluation. *Signal Process.*, 2005, **85**(9), 1859–1868.

12 **Rao, C., Ray, A., Sarkar, S.,** and **Yasar, M.** Review and comparative evaluation of symbolic dynamic filtering for detection of anomaly patterns. *Signal Image Video Process.*, 2008; DOI:10.1007/s11760-008-0061-8.

13 **Bennett, J., Kwong, K. S., Powell, C., Thomas, H.,** and **Krabbe, R.** An analysis of the causes of failure in high chrome oxide refractory materials from slagging gasifiers. US DOE/FE Report DOE/ARC-2005-008, 2006.

14 **Chen, E. S.** and **Buyukozturk, O.** Behavior of refractory linings for slagging gasifiers. MIT Report No. R84-07, Department of Civil Engineering, Massachusetts Institute of Technology, Cambridge, MA, USA, 1984.

15 **Watanabe, H.** and **Otaka, M.** Numerical simulation of coal gasification in entrained flow coal gasifier. *Fuel*, 2006, **85**, 1935–1943.

16 **Chen, C., Horio, M.,** and **Kojima, T.** Numerical simulation of entrained flow coal gasifiers. Part I: modeling of coal gasification in an entrained flow gasifier. *Chem. Eng. Sci.*, 2000, **55**, 3861–3874.

17 **Blond, E., Schmitt, N.,** and **Hild, F.** Response of saturated porous media to cyclic thermal loading. *Int. J. Numer. Anal. Methods Geomech.*, 2003, **27**, 883–904.

18 **Blond, E., Schmitt, N., Hild, F., Blumenfeld, P.,** and **Poirier, J.** Effect of slag impregnation on thermal degradations in refractories. *J. Am. Ceram. Soci.*, 2007, **90**(1), 154–162.

19 **Kokotovic, P., Khalil, H. K.,** and **O'Reilly, J.** *Singular perturbation methods in control analysis and design*, 1999 (Society of Industrial and Applied Mathematics, Philadelphia, PA, USA).

20 **Bockelie, M., Denison, M., Chen, Z., Linjewile, T., Senior, C., Sarofim, A.,** and **Holt, N.** CFD modeling for entrained flow gasifiers. San Francisco, CA, USA; 2002, available from http://www.gasification.org/Docs/Conferences/2002/GTC02039.pdf.

21 **Bockelie, M. J., Denison, M. K., Chen, Z., Linjewile, T., Senior, C. L.,** and **Sarofim, A. F.** CFD modeling for entrained flow gasifiers in Vision 21 Systems, 2003, available from http://reactioneng.com/downloads/REI_Bockelie_PCC_2002_Paper.pdf.

22 **Cundick, D. P., Blanchard, R. P., Maynes, D., Tree, D.,** and **Baxter, L. L.** Thermal transport to a reactor wall with a time varying ash layer. 5th US Combustion Meeting, San Diego, CA, USA, 2007, Paper #H11.

23 **Walsh, P. M., Sarofim, A. F.,** and **Beer, J. M.** Fouling of convection heat exchangers by lignitic coal ash. *Energy Fuels*, 1992, **6**, 709–715.

24 **Gupta, S.** and **Ray, A.** Pattern identification using lattice spin systems: a thermodynamic formalism. *Appl. Phys. Lett.*, 2007, **91**(19), 194105.

25 **Gupta, S., Ray, A.,** and **Keller, E.** Fatigue damage monitoring by ultrasonic measurements: a symbolic dynamics approach. *Int. J. Fatigue*, 2007, **29**(6), 1100–1114.

26 **Gupta, S., Ray, A.,** and **Mukhopadhyay, A.** Anomaly detection in thermal pulse combustors. *Proc. IMechE, Part I: J. Systems & Control Engineering*, 2006, **220**(5), 339–351.

27 **Pathria, R. K.** *Statistical mechanics*, 2nd edition, 1996 (Butterworth Heinemann, Oxford, UK).

28 **Lind, D.** and **Marcus, M.** *An introduction to symbolic dynamics and coding*, 1995 (Cambridge University Press, Cambridge, UK).

29 **Cover, T. M.** and **Thomas, J. A.** *Elements of information theory*, 1991 (John Wiley, New York, NY, USA).

30 **Buhl, M.** and **Kennel, M. B.** Statistically relaxing to generating partitions for observed time-series data. *Phys. Rev. E*, 2005, **71**(4), 046213.

31 **Mallat, S.** *A wavelet tour of signal processing*, 2nd edition, 1998 (Academic Press, Boston, MA, USA).

32 **Subbu, A.** and **Ray, A.** Space partitioning via Hilbert transform for symbolic time series analysis. *Appl. Phys. Lett.* 2008, **92**(8), 084107.

APPENDIX 1

Notation

$\mathcal{A}$	heat transfer area (m^2)
A, B	coefficients in the Weymann relation
Ash	total ash efflux at gasifier exit (kg/m^2s)
Cp	specific heat capacity (J/kg K)
g	acceleration due to gravity (m/s^2)
h	height of a compartment (m)
$\mathfrak{h}$	enthalpy (J/kg)
k	thermal conductivity (W/m K)
L	width of wall cross-section segment (m)
$\dot{M}_s^i$	slag mass deposition rate into the ith compartment from the combustion chamber (kg/m s)
$\dot{M}_s^{i,i+1}$	slag mass influx rate from the ith compartment into the $(i+1)$th compartment (kg/m s)
q	heat flux (J/m^2s)
r	radius, coordinate in the radial direction (m)
t	time (s)
T	temperature (K)
T_{cv}	critical solidification temperature for slag (K)
u	slag velocity in x-direction (m/s)
U_0	overall heat transfer coefficient (W/m^2 K)
z	coordinate in the axial direction (m)
α	thermal diffusivity (m^2/s)
ϵ	emissivity of the insulator wall
μ	viscosity (kg/ms)
ρ	slag density (kg/m^3)
σ	Stefan–Boltzmann constant ($W/m^2 K^4$)
τ	viscous shear stress for slag (kg/ms^2)

Subscripts and superscripts

AMB	ambient
cond	conduction
conv	convection
G	gaseous phase in combustor
gen	generation inside a compartment
i	ith compartment from top
in	energy/mass flow into a compartment
INS	insulator
int	edge between two successive compartments
LS	liquid slag
LSS	liquid slag surface
METAL	metal sheet
out	energy/mass flow out of a compartment
rad	radiation
REF	refractory
S	solid ash particles in combustor
SS	solid slag
tot	total efflux

APPENDIX 2

Review of symbolic dynamic filtering

This appendix briefly reviews the underlying concepts and salient features of SDF for detection of anomaly patterns (i.e deviations from the nominal condition) in complex dynamical systems [**4**]. The concept of SDF is built upon the principles borrowed from multiple disciplines including *statistical mechanics* [**24**, **27**], *symbolic dynamics* [**28**], *statistical pattern recognition* [**5**], and *information theory* [**29**]. SDF-based pattern recognition algorithms have been experimentally validated for real-time execution in different applications, such as electronic circuits [**11**, **12**] and fatigue damage monitoring in poly-crystalline alloys [**9**, **10**, **25**]. It has been shown by laboratory experimentation that SDF yields superior performance in terms of early detection of anomalies and robustness to measurement noise in comparison with other existing techniques

such as principal component analysis (PCA) and artificial neural networks (ANN) [**10–12**]. While the details are reported as pieces of information in previous publications [**4**, **7**, **25**, **26**], the essential concepts of space partitioning, symbol generation, and construction of a finite-state machine from the generated symbol sequence are succinctly explained in this appendix for the completeness of the paper.

Detection of anomaly patterns is formulated as a two-time-scale problem. The *fast time scale* is related to response time of the process dynamics. Over the span of a given time-series data sequence, dynamic behaviour of the system is assumed to remain invariant, i.e. the process is quasi-stationary at the fast time scale. In other words, the variations in the behaviour of system dynamics is assumed to be negligible on the fast time scale. The *slow time scale* is related to the time span over which parametric or non-parametric changes may occur and exhibit non-stationary dynamics. The concept of two time scales is illustrated in Fig. 9.

An observable non-stationary behaviour of the system dynamics can be associated with the anomalies evolving at a slow time scale. In general, a long time span in the fast time scale is a tiny (i.e. several order of magnitude smaller) interval in the slow time scale. For example, anomalies may evolve on the slow time scale in the order of tens of hours of operation; in contrast, the process dynamics may remain essentially invariant on the fast time scale in the order of minutes. Nevertheless, the notion of fast and slow time scales is dependent on the specific application, loading conditions, and operating environment. From the perspective of anomaly pattern detection, time-series data sets are collected on the fast time scale at different slow time epochs separated by uniform or non-uniform intervals.

Symbolic dynamics, encoding, and state machine

This section briefly describes the concepts of *symbolic dynamics*, encoding non-linear system dynamics from observed time-series data, and state machine construction for generation of symbol sequences. It also presents a procedure for online computation

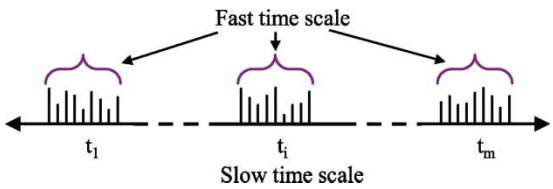

Fig. 9 Pictorial view of the two time scales: (i) *Slow time scale* of anomaly evolution and (ii) *Fast time scale* for data acquisition and signal conditioning

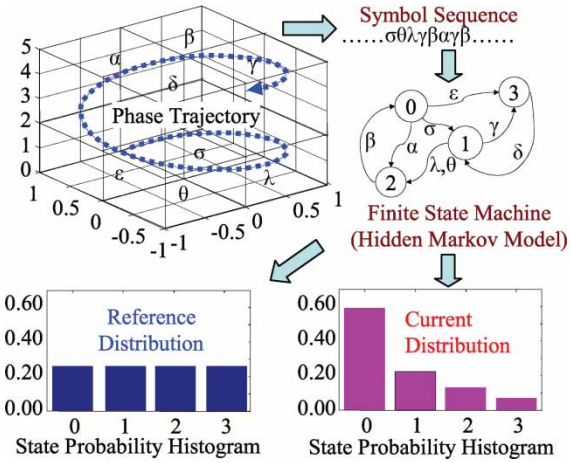

Fig. 10 Concept of SDF

of the machine state probability vectors that are representatives of the evolving patterns of the system's dynamical characteristics.

Let $\Omega \in \mathbb{R}^n$ be a compact (i.e. closed and bounded) region, within which the trajectory of the dynamical system is circumscribed as illustrated in Fig. 10. The region Ω is partitioned into a finite number of (mutually exclusive and exhaustive) cells, so as to obtain a coordinate grid. Let the cell, visited by the trajectory at a time instant, be denoted as a random variable taking a symbol value from the alphabet Σ. An orbit of the dynamical system is described by the time-series data as $\{x_0, x_1, \ldots, x_k, \ldots\}$ with $x_i \in \Omega$, which passes through or touches one of the cells of the partition. Each initial state $x_0 \in \Omega$ generates a sequence of symbols defined by a mapping from the phase space into the symbol space as

$$x_0 \rightarrow s_0 s_1 s_2 \cdots s_k \cdots \tag{19}$$

where each s_i $(i = 0, 1, \ldots)$ takes a symbol from the alphabet Σ. The mapping in equation (19) is called *symbolic dynamics* as it attributes a legal (i.e. physically admissible) sequence of symbols to the system dynamics starting from an initial state. Figure 10 pictorially elucidates the concepts of partitioning a finite region of the phase space and the mapping from the partitioned space into the symbol alphabet. This represents a spatial and temporal discretization of the system dynamics defined by the trajectories. Figure 10 also shows conversion of the symbol sequence into a finite-state machine as explained in the following subsections.

Space partitioning

A crucial step in SDF is partitioning of the phase space for symbol sequence generation [**4**]. Several partitioning techniques have been reported in literature for symbol generation [**30**], primarily based on symbolic

false nearest neighbours (SFNN), which may become cumbersome and extremely computation-intensive if the dimension of the phase space is large. Moreover, if the time-series data is noise-corrupted, then the symbolic false neighbours would rapidly grow in number and require a large symbol alphabet to capture the pertinent information on the system dynamics. Therefore, symbolic sequences as representations of the system dynamics should be generated by alternative methods because phase-space partitioning might prove to be a difficult task in the case of high dimensions and presence of noise. The wavelet transform [**31**] largely alleviates these shortcomings and is particularly effective with noisy data from high-dimensional dynamical systems. A comparison of wavelet partitioning and other partitioning methods, such as SFNN, is reported in recent literature, where wavelet space partitioning (WSP) [**7**] and analytic signal space partitioning (ASSP) [**32**] have been shown to yield comparable performance with several orders of magnitude smaller execution time. In either case, maximum entropy partitioning ensures the symbols of the alphabet to be uniformly distributed [**7**]. Once the partitioning of the data set at the nominal condition is completed, it is kept constant for all (slow time) epochs, i.e. the partitioning structure generated at the nominal condition serves as the reference frame for data analysis at subsequent slow time epochs.

State machine construction

The partitioning (Fig. 10) is performed at the slow time epoch t_0 of the nominal condition that is chosen to be the healthy state having zero anomaly measure. A finite-state machine is then constructed, where the states of the machine are defined corresponding to a given *alphabet* set Σ and window length D. The alphabet size $|\Sigma|$ is the total number of partition segments while the window length D is the length of consecutive symbol words [**4**], which are chosen as all possible words of length D from the symbol sequence. Each state belongs to an equivalence class of symbol words of length D or more, which is characterized by a word of length D at the leading edge.

The choice of $|\Sigma|$ and D depends on specific applications, noise level, and also on the available computation power. A large *alphabet* may be noise-sensitive and a small alphabet could miss the details of signal dynamics. Similarly, while a larger value of D is more sensitive to signal distortion, it would create a much larger number of states requiring more computation power.

The states of the machine are marked with the corresponding symbolic word permutation and the edges joining the states indicate the occurrence of a symbol σ_{i_ℓ}. The occurrence of a symbol at a state may keep the machine in the same state or move it to a new state. On a given symbol sequence $\cdots\sigma_{i_1}\sigma_{i_2}\cdots\sigma_{i_l}\cdots$ generated from the time-series data collected at a slow time epoch, a window of length D is moved by keeping a count of occurrences of word sequences $\sigma_{i_1}\cdots\sigma_{i_D}\sigma_{i_{D+1}}$ and $\sigma_{i_1}\cdots\sigma_{i_D}$ which are, respectively, denoted by $N(\sigma_{i_1}\cdots\sigma_{i_D}\sigma_{i_{D+1}})$ and $N(\sigma_{i_1}\cdots\sigma_{i_D})$. Note that if $N(\sigma_{i_1}\cdots\sigma_{i_D})=0$, then the state $q\equiv\sigma_{i_1}\cdots\sigma_{i_D}\in Q$ has zero probability of occurrence. For $N(\sigma_{i_1}\cdots\sigma_{i_D})\neq 0$, the transitions probabilities are then obtained by these frequency counts as follows

$$\pi_{jk}\equiv P(q_k|q_j)=\frac{P(q_k,q_j)}{P(q_j)}=\frac{P(\sigma_{i_1}\cdots\sigma_{i_D}\sigma)}{P(\sigma_{i_1}\cdots\sigma_{i_D})}$$
$$\Rightarrow \pi_{jk}\approx\frac{N(\sigma_{i_1}\cdots\sigma_{i_D}\sigma)}{N(\sigma_{i_1}\cdots\sigma_{i_D})} \tag{20}$$

where the corresponding states are denoted by $q_j\equiv\sigma_{i_1}\sigma_{i_2}\cdots\sigma_{i_D}$ and $q_k\equiv\sigma_{i_2}\cdots\sigma_{i_D}\sigma$. The state transition matrix, $\mathbf{\Pi}=[\pi]_{jk}$, satisfies the properties of a stochastic matrix, i.e. $\Sigma_k\pi_{jk}=1,\ \forall j$. The state probability vector $\boldsymbol{p}$ is derived as the left eigenvector of $\mathbf{\Pi}$ corresponding to the unity eigenvalue, which represents the behaviour pattern of the dynamical system at a given epoch.

Anomaly evolution and pattern identification

Behavioural pattern changes may take place in dynamical systems due to an accumulation of faults and progression of anomalies. The pattern changes are quantified as deviations from the nominal pattern (i.e. the state probability vector $\boldsymbol{p}^0$ at slow time epoch t_0). The resulting anomalies (i.e. deviations of the evolving patterns, $\boldsymbol{p}^k$ at epochs $t_k,\ k=1,2,\ldots,$ from the nominal pattern $\boldsymbol{p}^0$) are characterized by a scalar-valued function, called *anomaly measure* μ. The anomaly measures are obtained as

$$\mu_k\equiv d(\boldsymbol{p}^k,\boldsymbol{p}^0),\quad k=1,2,\ldots \tag{21}$$

where the $d(\bullet,\bullet)$ is an appropriately defined distance function.

The major advantages of SDF for the detection of small anomalies are listed below:

(a) robustness to measurement noise and spurious signals [**7**];
(b) adaptability to low-resolution sensing due to the coarse graining in space partitions [**4**];
(c) capability for early detection of anomalies because of sensitivity to signal distortion and real-time execution on commercially available inexpensive platforms [**25**].